Optics Letters

Whispering gallery germanium-on-silicon photodetector

Zhan Su,[1,3,*] Ehsan Shah Hosseini,[1,3] Erman Timurdogan,[1,3] Jie Sun,[1] Michele Moresco,[1] Gerald Leake,[2] Thomas N. Adam,[2] Douglas D. Coolbaugh,[2] and Michael R. Watts[1]

[1]Research Laboratory of Electronics, Massachusetts Institute of Technology, 77 Massachusetts Avenue, Cambridge, Massachusetts 02139, USA
[2]Colleges of Nanoscale Science and Engineering, State University of New York Polytechnic Institute, 257 Fuller Road, Albany, New York 12203, USA
[3]Current affiliation is Analog Photonics LLC, One Marina Park Drive, Boston, Massachusetts 02210, USA
*Corresponding author: zhansu@mit.edu

Received 10 May 2017; revised 18 June 2017; accepted 26 June 2017; posted 28 June 2017 (Doc. ID 295550); published 17 July 2017

We design and demonstrate, to the best of our knowledge, the first whispering gallery germanium-on-silicon photodetector with evanescent coupling from a silicon bus waveguide in a CMOS-compatible process. The small footprint (63.6 μm^2), high responsivity (~1.04 A/W at 1530 nm), low bias voltage (–1 V), low dark current (2.03 nA), and large optoelectric bandwidth (32.9 GHz) of the detector enable simultaneous wavelength filtering and power detection, ideal for handling large network data traffic. In addition, with the resonant nature of the detector, we also optimize the design to enable long-wavelength detection, achieving a separate device with a detection range of up to 1630 nm with a >0.45 A/W responsivity, making it an important building block for optical communication networks.

OCIS codes: (130.3120) Integrated optics devices; (230.5750) Resonators; (230.0250) Optoelectronics; (040.5160) Photodetectors.

https://doi.org/10.1364/OL.42.002878

Silicon photonics provides a promising solution to the ever-worsening bandwidth and power-consumption bottlenecks in both on- and off-chip interconnections [1]. The active participation of well-established complementary-metal-oxide-semiconductor (CMOS) foundries paves the way for custom fabrication processes tailored for large-scale electronics–photonics integration [2–6]. Thus far, near infrared photodetection has been achieved in a variety of materials, including germanium [7–13], polycrystalline silicon [14–16], silicon-germanium [17], III-V materials [18–21], and two-dimensional materials [22]. Among them, germanium has the advantages of efficient photocarrier generation and CMOS-compatible integration on silicon.

Germanium has a direct band gap of ~0.8 eV, making it a perfect photodetecting material for wavelengths below 1.55 μm. Sub-bandgap photodetections require an increase of detector sizes, in turn introducing a larger dark current and slowing detection speed. To achieve an efficient photodetection beyond 1.55 μm without compromising device performance, engineering material bandgaps with a strained germanium process was offered as a solution [7]. Demonstrations in guided optical devices were followed using butt- or evanescent-coupled detector designs [8–13]. However, for those designs, interaction lengths are still too short to enable efficient detection for longer wavelengths (e.g., L-band, 1565–1625 nm). This, however, can be compensated by using whispering-gallery-mode-based structures. While whispering gallery detectors have been demonstrated in polycrystalline silicon [14–16] and silicon-germanium [17] materials, their implementations in germanium-on-silicon photodetectors integrated on a silicon photonic platform are unexplored.

Here, we design and demonstrate the first whispering gallery germanium-on-silicon photodetector with evanescent coupling from the bus waveguide. The device has a 4.5-μm radius (area of 63.6 μm^2), a dark current as low as 2.03 nA (8.13 mA/cm^2 in germanium), and a peak responsivity of ~1.04 A/W at $\lambda \sim 1530$ nm when the detector is biased at –1 V. The compact size reduces the overall device capacitance without increasing resistance, resulting in a detection bandwidth of 32.9 GHz. The resonant nature further extends the detection wavelength range to 1630 nm with >0.45 A/W responsivity, enabling simultaneous detection of the S- (1460–1530 nm), C- (1530–1565 nm), and L-band (1565–1625 nm). In addition, owing to its wavelength-selective nature, both wavelength filtering and power detection functions are achieved with the same device, potentially simplifying the architecture for wavelength-division-multiplexing (WDM) and multicasting networks [23].

A schematic cross-section view of the whispering gallery germanium-on-silicon detector is shown in Fig. 1(a). The waveguide width is 400 nm to ensure a single-mode operation in the bus waveguide for wavelengths of around 1550 nm. ΔR_{Si-Ge} in Fig. 1(a) stands for the separation between the germanium and silicon outer radius. Silicon doping [bottom of Fig. 1(a)], intrinsic germanium (i-Ge), and germanium doping together form the *p-i-n* junction of the resonant detector. A doping concentration of ~$1e18/1e20$ cm^{-3} is used to form the lightly/highly doped silicon. For metal contacts to the germanium, circular contacts [24] are utilized to bring metal contacts close to where the carriers are generated, further reducing

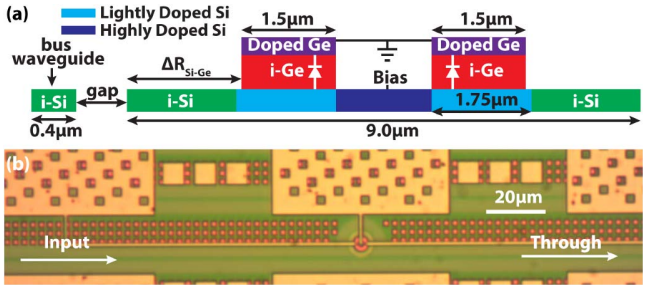

Fig. 1. (a) Schematic cross-sectional view of the whispering gallery germanium-on-silicon photodetector. ΔR_{Si-Ge} stands for the difference between germanium and silicon outer radius. (b) Top-view optical microscope image of the fabricated photodetector.

the device resistance. Input power from a bus waveguide is coupled into the resonator and absorbed by the cavity. The photodetector responsivity will be primarily limited by the ratio between the absorption of the intrinsic germanium that generates electron-hole pairs and other loss mechanisms such as radiation loss of the cavity design, doped silicon, and doped germanium absorptions. Radiation loss of the resonator is negligible with a 4.5-μm radius and high refractive index contrast between silicon (~3.48) and silicon dioxide (~1.44). To reduce doping-induced loss, the silicon underneath germanium is lowly doped to keep the absorption loss low while maintaining an efficient collection of the generated photocurrent. Through matching the external quality factor (Q factor) to the intrinsic Q factor of the cavity, power at the resonant wavelength can be fully coupled and absorbed with a high quantum efficiency.

The devices were fabricated on a 300-mm silicon-on-insulator wafer with a 220-nm silicon layer and a 2-μm buried oxide, using 193-nm optical immersion lithography. Germanium was hetero-epitaxially grown into the deep oxide trench on top of the thin silicon layer using a similar technique described in Ref. [3]. Figure 1(b) shows the top-view optical microscope image of the fabricated resonant detector.

The intrinsic Q factors of the resonators were calculated by fitting measured transmission spectra of a set of undercoupled resonant detectors to the coupled-mode-theory model [25]. Figure 2 shows the measured intrinsic Q factors of three transverse-electric (TE) modes (TE_{11}, TE_{21}, and TE_{31}) of different orders with different silicon-to-germanium separations (ΔR_{Si-Ge} = 1.0–2.0 μm). As the separation ΔR_{Si-Ge} gets

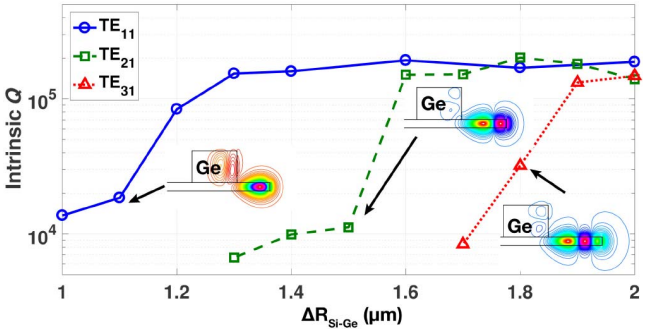

Fig. 2. Intrinsic Q factors for TE modes with different silicon and germanium outer-radius distances (ΔR_{Si-Ge}) for wavelength range of around 1530 nm. Inset: typical primary electric field distributions of TE_{11}, TE_{21}, and TE_{31} resonant modes.

smaller, the intrinsic Q factors of the modes in the cavity decrease, indicating increasing mode overlaps with germanium. The order of the mode also affects the mode overlap with the germanium as higher-order modes are less confined, resulting in germanium-absorption-limited intrinsic Q factors occurring at ΔR_{Si-Ge} = 1.1, 1.5, and 1.8 μm for TE_{11}, TE_{21} and TE_{31} modes, agreeing well with corresponding mode profiles (Fig. 2 insets).

I-V curves for germanium *p-i-n* diodes within resonant detectors with ΔR_{Si-Ge} = 1.1, 1.5, and 1.8 μm are measured, showing nA-scale dark current at −1 V bias voltage [Fig. 3(a)]. The dark current of the device with ΔR_{Si-Ge} of 1.1 μm is measured to be 2.03 nA at a −1 V bias voltage, corresponding to a dark current density of 8.13 mA/cm^2, comparable to the straight waveguide detector demonstrated in Ref. [3] that was fabricated using the same germanium recipe.

To characterize responsivities of the detectors, a TE-polarized tunable laser was edge-coupled in and out of the fabricated chip using single-mode fibers, and the transmission spectrum of the through port was recorded using an external detector. The coupling loss of the edge coupler is 4.3 dB/facet, and the coupling uncertainty is around ±0.05 dB. Silicon waveguide propagation loss of 2 dB/cm was included when calibrating the power into the detector. A ground-signal-ground high-speed probe was contacted to the device. A Keithley sourcemeter was used to bias the photodetector and measure the photocurrent at the same time. The transmission spectra together with the measured responsivity curves for different modes with a 100-nm bus-to-resonator gap are shown in Figs. 3(b)–3(d). When the wavelength of the input laser matches a resonance of the cavity, the light will be trapped and absorbed by the cavity. The light absorbed by the intrinsic germanium is converted to photocurrent, shown as photocurrent peaks in Figs. 3(b)–3(d). A responsivity as high as 1.04 A/W is achieved for the device with ΔR_{Si-Ge} = 1.5 μm and gap = 100 nm around the wavelength 1528 nm for mode TE_{21}. We also observed a responsivity of 0.80 A/W for both TE_{11} and TE_{31} for devices with 100-nm coupling gap, and ΔR_{Si-Ge} of 1.1 and 1.8 μm, respectively. Different optical full-width-half-maximum bandwidths (15, 50, and 22 GHz) were observed for modes with different orders, determined by the total Q factors of the resonant cavities [Figs. 3(b)–3(d) insets]. Figure 3(e) shows the responsivities of different modes for various ΔR_{Si-Ge} sizes with a 100-nm bus-to-resonator gap around the wavelength 1528 nm. Peak responsivities for different modes (e.g., 1.1 μm for TE_{11}, 1.5 μm for TE_{21}, and 1.7 μm for TE_{31}) are observed, corresponding to nearly critically coupled cases of individual modes. The measured responsivity is dependent on the Q-matching condition and the ratio between Ge absorption and other loss mechanisms (e.g., Si doping and Ge doping). For Q-matched cases and 100-nm coupling gap, TE_{21} provides the highest responsivity, indicating a larger ratio between Ge absorption and other loss mechanisms than that of TE_{11} and TE_{31} modes. With the resonant nature, the devices demonstrated here can also act as a wavelength-selective photodetector, combining wavelength filtering and signal-detecting functions. Furthermore, the structure can be optimized with a pulley-coupling scheme [17,26] to allow for a selective coupling to a certain mode while maintaining a relatively large coupling coefficient into the cavity. This will remove excitations of unwanted modes and extend the free

spectral range of the device. In addition, the current devices provide Lorentzian-type responsivity curves as a result of the first-order design. The roll-off speed can be improved with high-order designs by adding high-Q ring resonators between the bus waveguide and resonant detector.

To optimize the responsivity of the resonant detector, the external Q factor should match the intrinsic Q factor. Though the absorption coefficient of the i-Ge material decreases rapidly for longer wavelengths, the intrinsic Q factor of the resonator, including i-Ge absorption and other loss mechanisms, increases slowly as a result of mode expansions for longer wavelengths. This, in turn, makes it possible for a single device to maintain relatively high responsivities for both short (<1520 nm) and long wavelengths (>1580 nm) with a fixed bus-to-resonator gap. Figures 4(a)–4(c) show the responsivities for different resonant wavelengths and coupling gaps for $\Delta R_{\text{Si-Ge}}$ sizes of 1.1, 1.4, and 1.7 μm. For the device with $\Delta R_{\text{Si-Ge}} = 1.4$ μm and a coupling gap size of 100 nm, a responsivity as high as 0.8 A/W is achieved for short wavelength (~1480 nm) while a relatively high responsivity of 0.3 A/W for wavelengths of up to 1630 nm is also demonstrated. This agrees with our expectation that a large wavelength range detection can be achieved within a single device. With an optimized coupling gap, a responsivity as high as 0.45A/W is achieved for a wavelength of around 1630 nm for the device with $\Delta R_{\text{Si-Ge}} = 1.7$ μm and a coupling gap of 130 nm. Responsivities of the evanescent-coupled waveguide detector from Ref. [3] are also displayed in Figs. 4(a)–4(c) for comparison. We observe a more than 4 times increase in the responsivities for wavelengths longer than 1580 nm by using resonant germanium-on-silicon detectors.

We investigate the optoelectric bandwidth to determine the effects of photon lifetime, transit time, and RC bandwidth. The optoelectric bandwidth of the detector was measured using the heterodyne laser technique where two input lasers with the same power level and polarization but slightly different wavelengths are combined with a fiber-based 3 dB-coupler to generate GHz range beat frequencies at the on-chip detector.

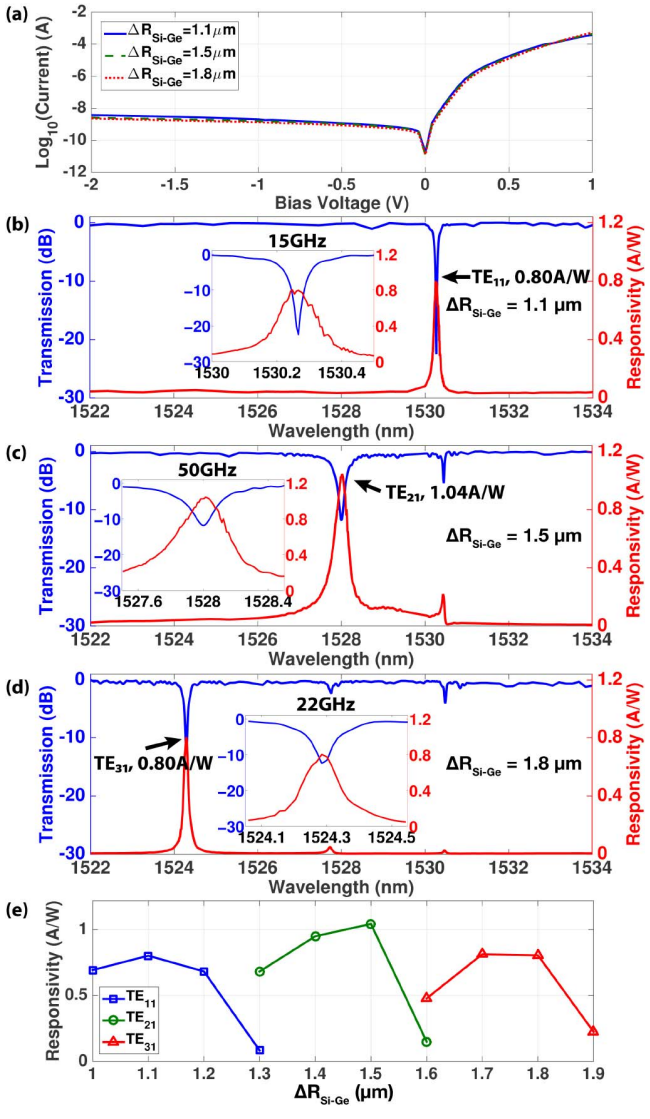

Fig. 3. (a) I-V curves of resonant detector with $\Delta R_{\text{Si-Ge}} = 1.1$, 1.5, and 1.8 μm, showing nA-scale dark current at −1 V bias voltage. (b)–(d) Transmission spectra and responsivities for resonant detectors with $\Delta R_{\text{Si-Ge}} = 1.1$, 1.5, and 1.8 μm at a bus-to-resonator gap of 100 nm for wavelength of around 1528 nm. Inset: zoom-ins around resonances, showing filter bandwidths of 15, 50, and 22 GHz. (e) Responsivities of devices with different $\Delta R_{\text{Si-Ge}}$ for modes TE_{11}, TE_{21}, and TE_{31} with a same 100-nm gap around a wavelength of 1528 nm.

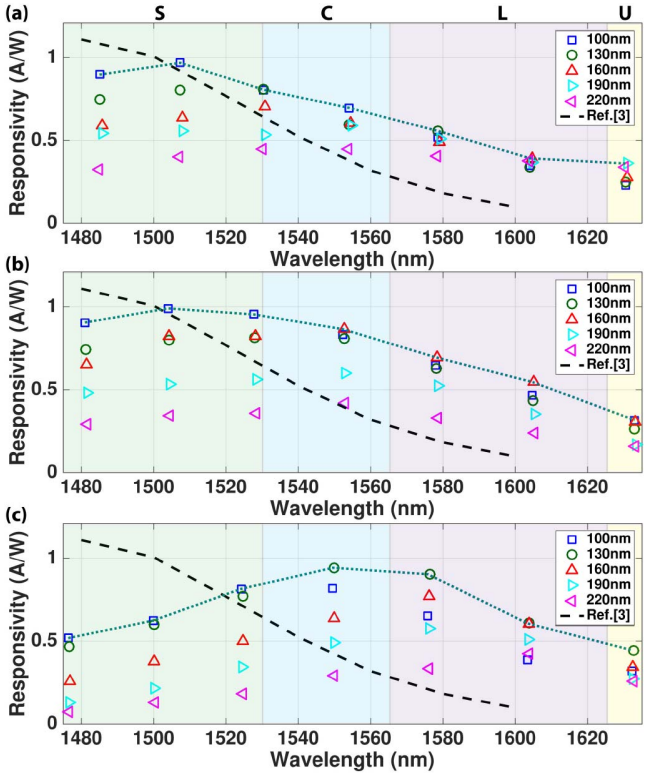

Fig. 4. Responsivities of the resonant detectors for different wavelengths and coupling gaps with (a) TE_{11}, $\Delta R_{\text{Si-Ge}} = 1.1$ μm. (b) TE_{21}, $\Delta R_{\text{Si-Ge}} = 1.4$ μm. (c) TE_{31}, $\Delta R_{\text{Si-Ge}} = 1.7$ μm. Evanescent-coupled waveguide detector responsivity curve (black-dashed line) from Ref. [3] is displayed here for comparison. Figures are shaded to mark different optical communication bands: S (1460–1530 nm), C (1530–1565 nm), L (1565–1625 nm), and U (1625–1675 nm).

Figure 5(a) shows measured bandwidths of the device with $\Delta R_{\text{Si–Ge}} = 1.5$ μm and a coupling gap of 100 nm for an input wavelength of around 1528 nm under different bias voltages. The bandwidth of the detector is improved from 1.2 GHz under zero bias to 32.9 GHz under −1 V or more bias voltages. Bandwidths for devices with a 100-nm coupling gap and different $\Delta R_{\text{Si–Ge}}$ sizes are shown in Fig. 5(b). For devices with $\Delta R_{\text{Si–Ge}} = 1.1$ μm and 1.8 μm, the measured bandwidths are 17.6 and 21.3 GHz, respectively, which are limited by the optical bandwidths or photon lifetime of the cavities (15 GHz for $\Delta R_{\text{Si–Ge}} = 1.1$ μm and 22 GHz for $\Delta R_{\text{Si–Ge}} = 1.8$ μm). However, for the device with $\Delta R_{\text{Si–Ge}} = 1.5$ μm, a bandwidth of 32.9 GHz was measured, less than the 50 GHz optical bandwidth [Fig. 3(c) inset] of the device. With the small footprint of the device, the bandwidth is not RC limited and is instead mainly limited by the transit time of the germanium material.

To summarize, we designed and demonstrated the first whispering gallery germanium-on-silicon detector with evanescent coupling from a silicon bus waveguide on an integrated silicon photonics platform. The compact size (63.6 μm^2), low dark current (∼2.03 nA), high responsivity (∼1.04 A/W), and high bandwidth (32.9 GHz) of the photodetector enable simultaneous wavelength filtering and power detection, suitable to handle large data traffic in a WDM network. In addition, with the resonant nature of the device, we also optimized the design for long-wavelength detection, achieving a separate device with 4 times better responsivity for a wavelength longer than 1580 nm than that of a straight detector fabricated using the same germanium recipe and an extended detection wavelength range of up to 1630 nm with a >0.45 A/W responsivity. This made it possible to handle the S-, C-, and L-band power detection using the same design.

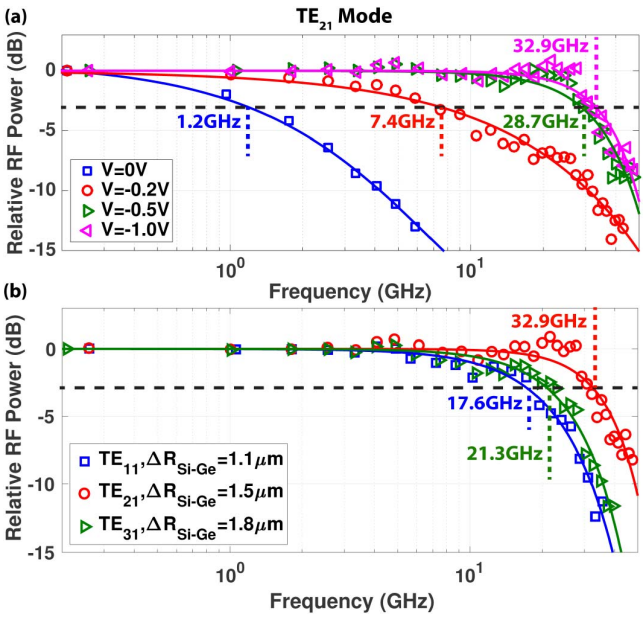

Fig. 5. (a) Measured bandwidths with different bias voltages for mode TE_{21}, device of $\Delta R_{\text{Si–Ge}} = 1.5$ μm, and gap = 100 nm, showing a 3 dB bandwidth of 32.9 GHz for −1 V bias voltage. (b) Measured bandwidths of devices with gap = 100 nm and $\Delta R_{\text{Si–Ge}}$ sizes of 1.1, 1.5, and 1.8 μm at −1 V bias voltage, showing bandwidths of 17.6, 32.9, and 21.3 GHz, respectively.

Funding. Defense Advanced Research Projects Agency (DARPA) (HR0011-12-2-0007).

REFERENCES

1. M. Asghari and A. V. Krishnamoorthy, Nat. Photonics **5**, 268 (2011).
2. J. Sun, E. Timurdogan, A. Yaacobi, E. S. Hosseini, and M. R. Watts, Nature **493**, 195 (2013).
3. E. Timurdogan, Z. Su, K. Settaluri, S. Lin, S. Moazeni, C. Sun, G. Leake, D. D. Coolbaugh, B. Moss, M. Moresco, V. Stojanović, and M. R. Watts, in *Optical Fiber Communication Conference Post Deadline Papers*, OSA Technical Digest (online) (Optical Society of America, 2015), paper Th5B.8.
4. C. Sun, M. T. Wade, Y. Lee, J. S. Orcutt, L. Alloatti, M. S. Georgas, A. S. Waterman, J. M. Shainline, R. R. Avizienis, S. Lin, B. R. Moss, R. Kumar, F. Pavanello, A. H. Atabaki, H. M. Cook, A. J. Ou, J. C. Leu, Y.-H. Chen, K. Asanović, R. J. Ram, M. A. Popović, and V. M. Stojanović, Nature **528**, 534 (2015).
5. F. Y. Liu, D. Patil, J. Lexau, P. Amberg, M. Dayringer, J. Gainsley, H. F. Moghadam, X. Zheng, J. E. Cunningham, A. V. Krishnamoorthy, E. Alon, and R. Ho, IEEE J. Solid-State Circuits **47**, 2049 (2012).
6. Z. Su, N. Li, E. S. Magden, M. Byrd, P. Purnawirman, T. N. Adam, G. Leake, D. Coolbaugh, J. D. B. Bradley, and M. R. Watts, Opt. Lett. **41**, 5708 (2016).
7. J. Michel, J. Liu, and L. C. Kimerling, Nat. Photonics **4**, 527 (2010).
8. D. Feng, S. Liao, P. Dong, N. N. Feng, H. Liang, D. Zheng, C. C. Kung, J. Fong, R. Shafiiha, J. Cunningham, A. V. Krishnamoorthy, and M. Asghari, Appl. Phys. Lett. **95**, 261105 (2009).
9. A. Novack, M. Gould, Y. Yang, Z. Xuan, M. Streshinsky, Y. Liu, G. Capellini, A. E.-J. Lim, G.-Q. Lo, T. Baehr-Jones, and M. Hochberg, Opt. Express **21**, 28387 (2013).
10. L. Vivien, A. Polzer, D. Marris-Morini, J. Osmond, J. M. Hartmann, P. Crozat, E. Cassan, C. Kopp, H. Zimmermann, and J. M. Fédéli, Opt. Express **20**, 1096 (2012).
11. C. T. DeRose, D. C. Trotter, W. A. Zortman, A. L. Starbuck, M. Fisher, M. R. Watts, and P. S. Davids, Opt. Express **19**, 24897 (2011).
12. G. Li, Y. Luo, X. Zheng, G. Masini, A. Mekis, S. Sahni, H. Thacker, J. Yao, I. Shubin, K. Raj, J. E. Cunningham, and A. V. Krishnamoorthy, Opt. Express **20**, 26345 (2012).
13. S. Liao, N. N. Feng, D. Feng, P. Dong, R. Shafiiha, C. C. Kung, H. Liang, W. Qian, Y. Liu, J. Fong, J. E. Cunningham, Y. Luo, and M. Asghari, Opt. Express **19**, 10967 (2011).
14. D. F. Logan, P. Velha, M. Sorel, R. M. De La Rue, A. P. Knights, and P. E. Jessop, IEEE Photon. Technol. Lett. **22**, 1530 (2010).
15. K. Preston, Y. H. D. Lee, M. Zhang, M. Zhang, and M. Lipson, Opt. Lett. **36**, 52 (2011).
16. K. K. Mehta, J. S. Orcutt, J. M. Shainline, O. Tehar-Zahav, Z. Sternberg, R. Meade, M. A. Popović, and R. J. Ram, Opt. Lett. **39**, 1061 (2014).
17. L. Alloatti and R. J. Ram, Appl. Phys. Lett. **108**, 071105 (2016).
18. J. Brouckaert, G. Roelkens, D. Van Thourhout, and R. Baets, J. Lightwave Technol. **25**, 1053 (2007).
19. H. Park, A. W. Fang, R. Jones, O. Cohen, O. Raday, M. N. Sysak, M. J. Paniccia, and J. E. Bowers, Opt. Express **15**, 6044 (2007).
20. Z. Sheng, L. Liu, J. Brouckaert, and S. He, Opt. Express **18**, 1756 (2010).
21. D. K. T. Ng, Q. Wang, J. Pu, K. P. Lim, Y. Wei, Y. Wang, Y. Lai, and S. T. Ho, Opt. Lett. **38**, 5353 (2013).
22. F. H. L. Koppens, T. Mueller, P. Avouris, A. C. Ferrari, M. S. Vitiello, and M. Polini, Nat. Nanotechnol. **9**, 780 (2014).
23. Z. Su, M. Cherchi, E. Timurdogan, J. Sun, M. Moresco, G. Leake, D. Coolbaugh, and M. R. Watts, Opt. Lett. **39**, 5459 (2014).
24. E. Timurdogan, C. M. Sorace-Agaskar, J. Sun, E. S. Hosseini, A. Biberman, and M. R. Watts, Nat. Commun. **5**, 4008 (2014).
25. H. Haus and W. P. Huang, Proc. IEEE **79**, 1505 (1991).
26. J. M. Shainline, J. S. Orcutt, M. T. Wade, K. Nammari, B. Moss, M. Georgas, C. Sun, R. J. Ram, V. Stojanović, and M. A. Popović, Opt. Lett. **38**, 2657 (2013).